RSC Advances

ROYAL SOCIETY OF CHEMISTRY

PAPER

View Article Online
View Journal | View Issue

Cite this: *RSC Adv.*, 2025, **15**, 5507

Boronic acid-functionalized Fe_3O_4 nanoparticles for activity-preserved enrichment of low-abundance bacteria from real samples†

Jingwen Chen,[ab] Shaobo Li,[ab] Bin Deng,[ab] Hongyuan Wang,[ab] Wenkui Sun,[c] Li Li,[*b] Zongchun Bai*[b] and Jing Liu[*a]

Pathogenic bacterial infections represent a significant and ongoing threat to public health. The development of a sensitive, convenient, and accurate method for diagnosing pathogenic bacteria is a formidable challenge due to their low abundance in complex biological samples, especially in the early stages of diseases. In this study, a kind of phenylboronic acid-functionalized Fe_3O_4 nanoparticles (NPs), known as Fe_3O_4@poly(PEGDA-*co*-MAAPBA) NPs, was developed for effectively enriching low levels of pathogenic bacteria from complex samples and then diagnosing them through microbiological cultures. In this design, the resultant Fe_3O_4@poly(PEGDA-*co*-MAAPBA) NPs could recognize pathogenic bacteria because of the reversible reactions between the phenylboronic acid groups on the NPs and the *cis*-diol structures outside of the bacterial cells. By exploiting the magnetic properties of Fe_3O_4 NPs, bacteria were able to anchored onto the resulting NPs (NPs@bacteria) for easy enrichment. Utilizing microbiological culture techniques, successful cultivation of NPs@bacteria was achieved, demonstrating that bacterial activity remained unaffected during the enrichment process. The proposed method exhibited a limit of detection as low as 0.4 colony-forming units per milliliter. The Fe_3O_4@poly(PEGDA-*co*-MAAPBA) NPs were applied successfully for testing *Staphylococcus aureus* in urine samples which were typically considered to be free of bacterial contamination, indicating excellent selectivity and enrichment capability of the prepared NPs in complex samples. It suggests that the Fe_3O_4@poly(PEGDA-*co*-MAAPBA) NPs have the potential to become a powerful tool for early diagnosis of pathogenic bacteria in the clinic.

Received 17th December 2024
Accepted 10th February 2025

DOI: 10.1039/d4ra08826c

rsc.li/rsc-advances

Introduction

Pathogenic bacterial infections can result in the development of serious diseases and, in some cases, death in humans. This poses a significant threat to public health and the global economy.[1–3] Therefore, the detection of pathogenic bacteria at low concentrations in complex samples is essential to minimize the associated risks.

Currently, there are several diagnostic methods for identifying pathogenic bacterial infections, including microbiological cultures, enzyme-linked immunosorbent assay (ELISA), polymerase chain reaction (PCR)-based tests, and various functional NPs.[4–6] Among them, the microbiological culture technique is regarded as the "golden standard" for bacterial diagnosis. However, it has a relatively higher limit of detection (LOD) of around 30 colony-forming units per milliliter (CFU mL^{-1}). In the early stage of a pathogenic bacterial infection, the concentration of bacteria in the body fluids of the infected individual, such as blood, urine, or sweat, might be lower than the LOD value of microbiological culture technology, which will result in a delay in the diagnosis of pathogenic bacteria. As the infection progresses to a more serious stage, the concentration of bacteria in the body fluids of the infected reaches a level sufficient for culturing. Pathogenic bacterial diagnosis typically takes 24–72 hours, given the inherent complexity and time-consuming nature of microbiological culture technology. It is an inevitable delay in controlling the pathogenic bacterial infection and, in some cases, will increase the death rate in patients. PCR has the potential to offer rapid and accurate detection of pathogenic bacteria with a lower LOD. However, its application is constrained by the labor-intensive and complex procedures, the requirement for professional expertise, and the high cost of equipment. ELISA is one of the widely used

[a]*School of Pharmacy, China Pharmaceutical University, No. 24 Tongjiaxiang Road, Nanjing, 210009, China. E-mail: liujing@cpu.edu.cn*

[b]*Institute of Agricultural Facilities and Equipment, Jiangsu Academy of Agricultural Sciences, Key Laboratory of Protected Agriculture Engineering in the Middle and Lower Reaches of Yangtze River, Ministry of Agriculture and Rural Affairs, 50 Zhongling Street, Nanjing 210014, China. E-mail: muzishuiqudou@163.com; vipmaple@126.com*

[c]*Department of Respiratory and Critical Care Medicine, the First Affiliated Hospital of Nanjing Medical University, No. 300 Guangzhou Road, Nanjing, 210029, China*

† Electronic supplementary information (ESI) available. See DOI: https://doi.org/10.1039/d4ra08826c

methods for bacterial diagnosis due to its user-friendly nature, convenience, and affordability. Nevertheless, the limited availability of specific antibodies for certain bacteria restricts the effectiveness of ELISA in bacterial diagnosis.[7–11]

Recently, the development of diverse functional NPs has emerged as a promising tool for diagnosing pathogenic bacteria.[12–15] Among NPs, the functional bio-recognition element plays a crucial role in diagnosing pathogenic bacteria, typically consisting of a biomolecule like an antibody, enzyme, cell, or nucleic acid.[16–20] Immune NPs, one of the most widely used NPs, have been restricted in applications in diagnosing pathogenic bacteria due to the limited availability of specific antibodies for certain bacteria.[12,21] Furthermore, antibodies, enzymes, cells, and nucleic acids are highly susceptible to environmental degradation.[22] Therefore, these bio-recognition elements modified NPs are constrained by instability as well as the high cost of the development of biomolecules. Hence, many researchers have focused on developing rapid, sensitive, convenient, and accurate methods for the determination of pathogenic bacteria from complex samples.

Given the challenges posed by serious pathogenic bacterial infections and developing novel determination methods, we proposed a new strategy for determining low concentrations of pathogenic bacteria. This involved the enrichment of live bacteria from complex samples and subsequent diagnosis of them using classical diagnostic methods. In recent years, phenylboronic acid and its derivatives have attracted attention as recognition molecules for the detection of bacteria due to their selective binding with *cis*-diol groups on the surface of bacteria in an alkaline aqueous solution.[23–27] The stable interaction between the phenylboronic acid and bacteria can be dissociated when the environmental pH is switched to acidic.[28,29] Functional Fe_3O_4 nanoparticles (NPs) have been commonly employed for the separation or enrichment of pathogenic bacteria from complex samples because of their favorable superparamagnetism, excellent monodispersity, prompt magnetic reactivity, good biocompatibility, and relatively low cost of preparation.[30–34] In light of the merits of magnetic NPs and the rapid development of bio-orthogonal techniques, we designed phenylboronic acid-functionalized magnetic NPs for the rapid capture of live bacteria from complex samples, thereby improving the sensitivity of diagnosis.

In this work, 3-methacrylamidophenylboronic acid (MAAPBA), a widely employed phenylboronic acid monomer, was utilized as the functional monomer for reversible binding *cis*-diol groups on the surface of bacteria. Poly(ethylene glycol) diacrylate (PEGDA), a water-soluble cross-linker, was used as the primary material for cross-linking the functional monomer and capping the magnetic NPs (MNPs). As illustrated in Scheme 1, Fe_3O_4 NPs synthesized *via* the solvothermal method were modified with silane reagents to introduce double bonds onto their surface, and subsequently copolymerized with the phenylboronic acid monomer MAAPBA and the cross-linker PEGDA, forming the Fe_3O_4@poly(PEGDA-*co*-MAAPBA) NPs. The developed Fe_3O_4@poly(PEGDA-*co*-MAAPBA) NPs successfully demonstrated that they could selectively capture and concentrate bacteria through boronate affinity in an alkaline aqueous environment. Furthermore, the complex

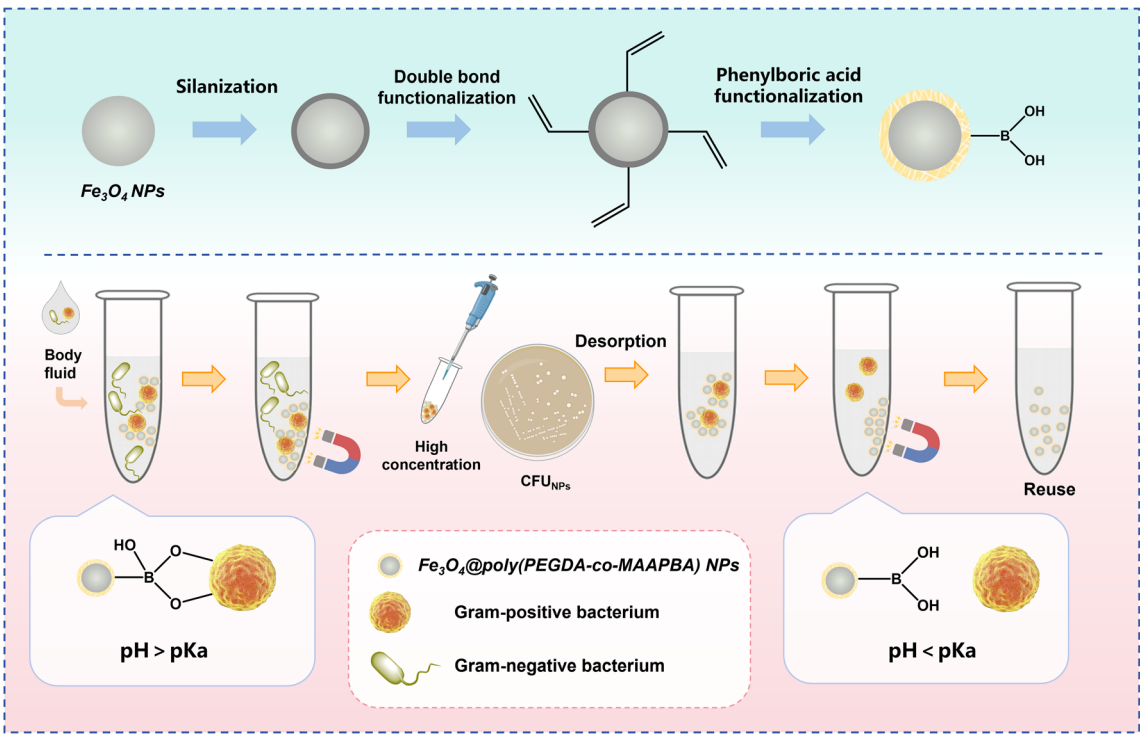

Scheme 1 Schematic illustration of the synthesis steps of the phenylboronic acid-functionalized Fe_3O_4 nanoparticles (Fe_3O_4@poly(PEGDA-*co*-MAAPBA) NPs), and the applications in enriching and diagnosing low abundances of pathogenic bacteria.

NPs@bacteria could be cultivated and diagnosed using the conventional culture-based method. As a result, the Fe_3O_4@-poly(PEGDA-*co*-MAAPBA) NPs exhibited good biocompatibility, relatively low cost of preparation, excellent enrichment ability, and reusability, successfully performing the enrichment of low concentrations Gram-positive bacteria in the complex samples and enhancing the sensitivity of classical diagnostic methods.

Materials and methods

Materials and reagents

3-Methacrylamidophenylboronic acid (MAAPBA), tetraethoxysilane (TEOS), 2,2′-azobis(2-methylpropionitrile) (AIBN), and poly(ethylene glycol) 200 (PEG 200) were purchased from Macklin Biochemical Co., Ltd. (Shanghai, China). 3-(Triethoxysilyl) propyl methacrylate (TPM), phosphate buffer saline (PBS) buffer (pH 7.4), artificial intestinal Fluid (sterile), LB broth medium, and LB agar medium were obtained from Shanghai Yuanye Biotechnology Co., Ltd. (Shanghai, China). Poly(-ethylene glycol) diacrylate (PEGDA) was purchased from Shanghai Aladdin Biochemical Technology Co., Ltd. (Shanghai, China). Hexahydrate ferric chloride ($FeCl_3 \cdot 6H_2O$), sodium hydroxide (NaOH), sodium acetate (NaAc), anhydrous ethanol, acetic acid, polyvinyl alcohol (PVA), trisodium citrate dihydrate, and surfactant-free cellulose acetate membrane filters (pore size 0.22 μm) were purchased from Sinopharm Reagent Company (Shanghai, China). *Staphylococcus aureus* (*S. aureus*) ATCC 29213 and *Escherichia coli* (*E. coli*) ATCC 25922 were purchased from Vita Chemical Reagent Co., Ltd. (Shanghai, China). *Salmonella typhimurium* (*S. typhimurium*), *Staphylococcus haemolyticus* (*S. haemolyticus*), *Pasteurella multocida* (*P. multocida*), and *Streptococcus uberis* (*S. uberis*) were obtained from College of Veterinary Medicine, Yangzhou University. SYTO9-PI Live and Dead Bacteria Stain Kits were purchased from Beijing Tianjingsha Gene Technology Co., Ltd. (Beijing, China). All chemical reagents were analytical reagent grade unless specially mentioned. Water used in experimental work was purified using the MZY-U10 ultra-pure water system (Miaozhiyi Electronic Technology Co. Ltd., Nanjing, China).

Synthesis of Fe_3O_4@poly(PEGDA-*co*-MAAPBA) NPs

The synthetic procedure for Fe_3O_4@poly(PEGDA-*co*-MAAPBA) NPs is shown in Fig. 1. The phenylboronic acid-functionalized Fe_3O_4 NPs were prepared through a two-step strategy: the preparation of double-bond functionalized Fe_3O_4 NPs, and the copolymerization of cross-linker PEGDA, functional monomer MAAPBA, and double-bond functionalized Fe_3O_4 NPs.

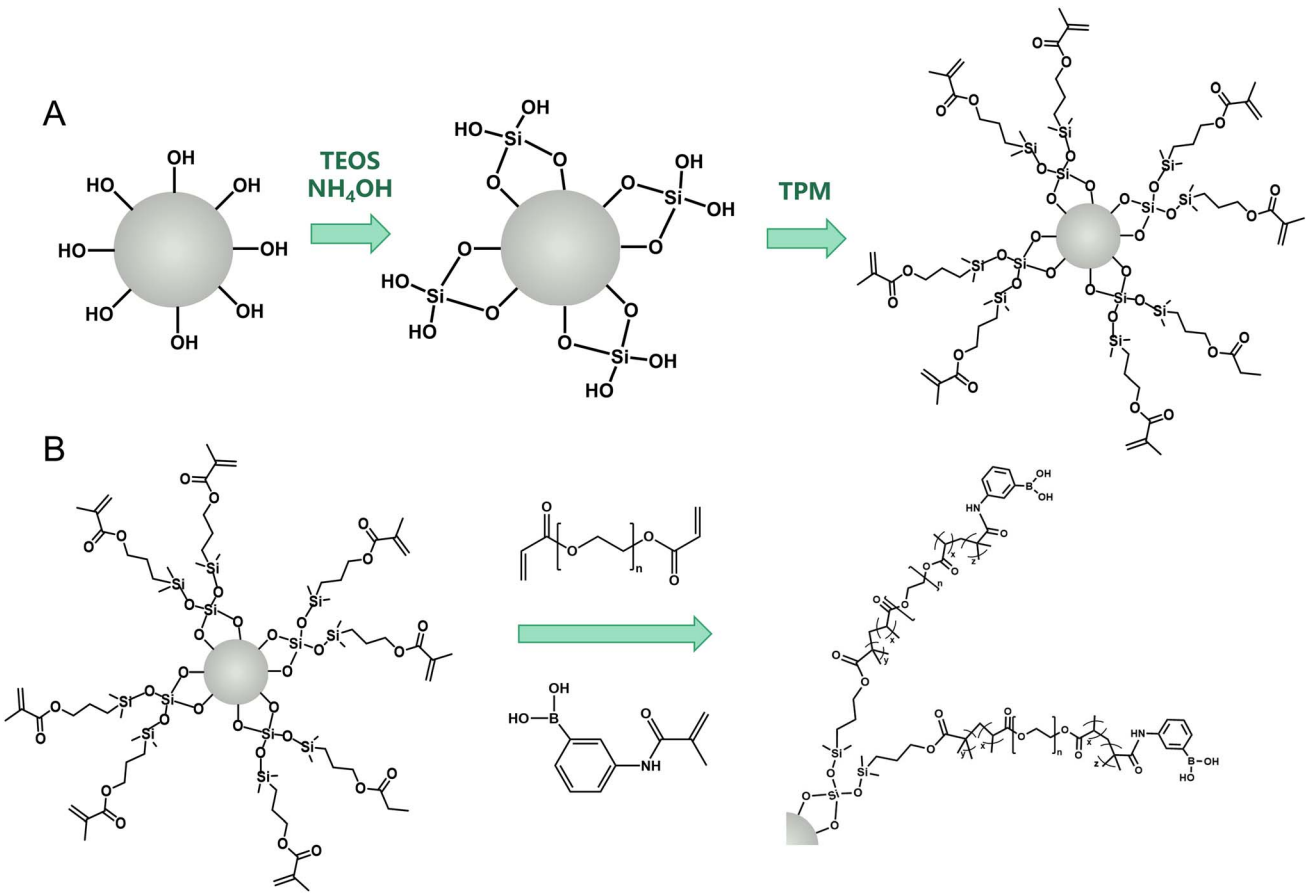

Fig. 1 Schematic illustration of the synthesis method of Fe_3O_4@poly(PEGDA-*co*-MAAPBA) NPs. The phenylboronic acid-functionalized Fe_3O_4 NPs were prepared through a two-step strategy: (A) the preparation of double-bond functionalized Fe_3O_4 NPs, and (B) the copolymerization of double-bond functionalized Fe_3O_4 NPs, cross-linker PEGDA, and functional monomer MAAPBA.

Fe_3O_4 NPs were synthesized by the solvothermal method.[35] Briefly, 1.1 g of $FeCl_3 \cdot 6H_2O$ was dissolved in 42 mL of ethylene glycol. After stirring for 30 min at 600 rpm, 2.7 g NaAc, and 0.6 g trisodium citrate dihydrate were added with continuous stirring for 1 h. Next, the solution was transferred into an autoclave at 200 °C for 12 h. Then, Fe_3O_4 NPs were isolated through a magnet. After washing extensively with water and ethanol, the obtained products were vacuum-dried at 50 °C for 12 h and stored in the vacuum for further experiments.

The double-bond functionalized Fe_3O_4 NPs were synthesized first by capping the Fe_3O_4 NPs to form the Fe_3O_4@SiO_2 NPs. Briefly, 500 mg of the prepared Fe_3O_4 NPs were dispersed in 250 mL of anhydrous ethanol with ultrasonic dispersion for 30 min. Then, the mixture was transferred to a water bath at 50 °C and stirred for 10 min at 1200 rpm. While maintaining continuous stirring, 4 mL of TEOS ethanol (v : v = 1 : 1) was added dropwise again [36]. After continuous stirring for 1 h, the Fe_3O_4@SiO_2 NPs were collected through a magnet and washed with large amounts of water and ethanol to remove the unreacted TEOS. Next, the obtained Fe_3O_4@SiO_2 NPs and 7.5 mL of TPM were dispersed in 250 mL of anhydrous ethanol at 80 °C with stirring at 1200 rpm for 8 h in the dark.[37] Then, the obtained double-bond functionalized Fe_3O_4 NPs were collected through a magnet. After washing with large amounts of water and ethanol, the obtained products were vacuum-dried at 50 °C for 12 h and stored in the vacuum for further experiments.

The Fe_3O_4@poly(PEGDA-*co*-MAAPBA) NPs were synthesized using the thermal polymerization.[38–40] Briefly, certain amounts of MAAPBA, 0.1 g of the obtained double-bond functionalized Fe_3O_4 NPs, 0.8 mL of PEG 200, and 0.2 mL of PEGDA were dispersed in 40 mL of PVA aqueous solution (1% w/v) with a 1200 rpm stirring at 70 °C. Keep stirring, and 0.4 mL of the 3% AIBN solution dissolved in PEG 200 (w/v) was added. After stirring for 8 h at 70 °C, the mixture was cooled to room temperature, and the product was collected through a magnet. After washing with large amounts of water and ethanol, the obtained resultant products were vacuum dried at 50 °C for 12 h and stored in the vacuum for further experiments. The mass ratios of MAAPBA to PEGDA were 1 : 200, 1 : 100, 1 : 50, 1 : 10, and 1 : 5, and the products were named herein as S2, S3, S4, S5, and S6, respectively. The obtained Fe_3O_4@poly(PEGDA) NPs using the same step without adding MAAPBA were named S1 herein.

Zeta potentials and particle sizes of the prepared NPs

The zeta potentials and particle sizes of the prepared NPs were characterized using a Malvern Zetasizer Nano ZS90 instrument at 25 °C with a scattering angle of 90°. The aqueous solution of NPs at 0.5 mg mL^{-1} was prepared to accurately measure their surface charges and particle sizes.

Culturing of bacteria

Specific amounts of *S. aureus*, *E. coli*, *S. typhimurium*, or *S. haemolyticus* were cultured in 1 mL of sterilized LB broth medium at 37 °C for 24 h with shaking at 200 rpm. Specific amounts of *S. uberis* or *P. multocida* strains were cultured in 1 mL of sterilized Todd Hewitt broth medium at 37 °C for 24 h with shaking at 200 rpm. After that, 100 μL of the prepared bacterial cultures were dispersed in the sterilized PBS buffer (10 mM, pH 7.4), forming the corresponding bacterial PBS suspensions with approximately 10^8 CFU mL^{-1}.

SEM images

The micromorphology of the optimal Fe_3O_4@poly(PEGDA-*co*-MAAPBA) NPs, *E. coli* (ATCC 25922) and *S. aureus* (ATCC 29213) cells before and after treatment with the functionalized NPs was investigated by SEM (EVO-LS10, ZEISS, Oberkochen, Germany). For sample preparation, 2 mg of sterilized Fe_3O_4@poly(PEGDA-*co*-MAAPBA) NPs and 20 μL of NaOH aqueous solution (0.1 M) were dispersed in 1 mL of *E. coli* or *S. aureus* PBS suspension (approximately 10^8 CFU mL^{-1}, the bacterial PBS suspension was prepared according to the procedure shown in the Section Culturing of Bacteria). After incubation in a bacterial culture room at 37 °C with shaking at 200 rpm for 30 min, the Fe_3O_4@poly(PEGDA-*co*-MAAPBA) NPs were collected through a magnet. After that, the collected Fe_3O_4@poly(PEGDA-*co*-MAAPBA) NPs were washed three times with large amounts of sterilized PBS buffer and dispersed in 1 mL of PBS buffer. Next, the prepared solution of NPs and *E. coli* and *S. aureus* PBS suspensions without treatment with Fe_3O_4@poly(PEGDA-*co*-MAAPBA) NPs were dropped onto the surface of the conductive glass, lyophilized, and coated with an 8 nm-thick gold film. SEM images acquired under high vacuum conditions.

Live/dead staining test

After treatment with or without the optimal Fe_3O_4@poly(PEGDA-*co*-MAAPBA) NPs, the PBS suspension of *S. aureus* with around 10^8 CFU mL^{-1} was stained with SYTO9 and propidium iodide (PI) for 15 min in the dark. IX-51 Fluorescent inverted microscope (Olympus Corporation, Japan) was used to observe live bacteria (green fluorescence) and dead bacteria (red fluorescence).[41]

CFU counting method

Firstly, a series of bacterial PBS solutions containing *E. coli*, *S. typhimurium*, *S. aureus*, *S. haemolyticus*, *S. uberis*, or *P. multocida* with different concentrations from 0–10^3 CFU mL^{-1} were prepared by diluting the corresponding bacterial PBS suspensions (approximately 10^8 CFU mL^{-1}, prepared according to the procedure shown in the Section Culturing of Bacteria). Next, 100 μL of the *S. aureus*, *E. coli*, *S. typhimurium*, or *S. haemolyticus* PBS solution (concentrations from 0–10^3 CFU mL^{-1}) was spread aseptically on the LB nutrient agar plate. 100 μL of the *S. uberis* or *P. multocida* PBS solution (concentrations from 0–10^3 CFU mL^{-1}) was spread aseptically on the blood agar plate. These plates were then incubated in a bacterial culture room for 24 h at 37 °C. Images of the plates were captured, and the colony count was counted. All the experiments were carried out in triplicate.[42]

Turbidity test

Certain amounts of sterilized Fe_3O_4@poly(PEGDA-*co*-MAAPBA) NPs (0–8 mg) and 40 μL of NaOH aqueous solution (0.1 M) were

dispersed in 2 mL of *E. coli* or *S. aureus* PBS suspension (approximately 10^8 CFU mL^{-1}, the bacterial suspension was prepared according to the procedure shown in the Section Culturing of Bacteria). After stirring for 30 min, the Fe_3O_4@poly(PEGDA-*co*-MAAPBA) NPs were anchored at the bottom by a magnet, and the optical densities of the suspensions at 600 nm were measured using the NanoDrop 2000 instrument (Thermo Scientific, Waltham, MA, USA). *E. coli* or *S. aureus* PBS suspension without the treatment of Fe_3O_4@poly(PEGDA-*co*-MAAPBA) NPs was used as the control. All experiments were performed in triplicate.

Enrichment test

1.5 mg of sterilized Fe_3O_4@poly(PEGDA-*co*-MAAPBA) NPs and 1 mL of NaOH aqueous solution (0.1 M) were dispersed in 50 mL of *S. aureus*, *S. haemolyticus*, or *S. uberis* PBS suspension (approximately 10^1 CFU mL^{-1}). After stirring for 30 min, the Fe_3O_4@poly(PEGDA-*co*-MAAPBA) NPs were anchored at the bottom by a magnet, and the supernatant was removed. Then, 100 μL of PBS buffer was added to form the NP suspension. After that, the 100 μL suspension with Fe_3O_4@poly(PEGDA-*co*-MAAPBA) NPs was spread on a nutrient agar plate. These plates were then incubated in a bacteria-culture room for 24 h at 37 °C. Images of the plates were captured, and the colony count was counted. All the experiments were carried out in triplicate.

Reusability test

0.6 mg of sterilized Fe_3O_4@poly(PEGDA-*co*-MAAPBA) NPs and 20 μL of NaOH aqueous solution (0.1 M) were dispersed in 1 mL of *S. aureus* PBS suspension (approximately 10^3 CFU mL^{-1}). After stirring for 30 min, the Fe_3O_4@poly(PEGDA-*co*-MAAPBA) NPs were anchored at the bottom by a magnet, 100 μL of the supernatant was used to count the colony count using the CFU method, and 1 mL of PBA buffer was used to wash these NPs three times. Then, 1 mL of acetic acid solution (0.1 M, pH 2.7) was used to dissociate *S. aureus* from the NPs, and 1 mL of PBS buffer was used to wash them three times. After that, these Fe_3O_4@poly(PEGDA-*co*-MAAPBA) NPs were used to capture and dissociate *S. aureus* until the fifth cycle was completed in the same way.

Detection of bacteria in complex samples

S. aureus, *S. haemolyticus*, or *S. uberis* PBS suspension (approximately 10^8 CFU mL^{-1}) was diluted with simulated intestinal fluid to form the complex samples with a concentration of approximately 10^2 CFU mL^{-1}. Then, 0.6 mg of sterilized Fe_3O_4@poly(PEGDA-*co*-MAAPBA) NPs and 20 μL of NaOH aqueous solution (0.1 M) were dispersed in 1 mL of the prepared complex samples. After stirring for 30 min, the Fe_3O_4@poly(PEGDA-*co*-MAAPBA) NPs were magnetically separated. 100 μL of supernatant was collected for colony counting, and 1 mL of PBS buffer was used to wash these NPs three times. Then, 100 μL of PBS buffer was added to form the NP suspension. After that, the NP suspension was spread on a nutrient agar plate, and the plate was incubated in a bacteria-culture room for 24 h at 37 °C. Images of the plates were captured, and the colony count was determined. All the experiments were carried out in triplicate.

100 μL of *S. aureus* or *S. haemolyticus* suspension (approximately 10^2 CFU mL^{-1}) and 100 μL of *E. coli* suspension (approximately 10^4 CFU mL^{-1}) were diluted using 25 mL of urine contributed by a healthy female volunteer to form the real samples with a concentration of approximately 0.4 CFU mL^{-1} of *S. aureus* or *S. haemolyticus* and 40 CFU mL^{-1} of *E. coli*. Then, 1 mg of sterilized Fe_3O_4@poly(PEGDA-*co*-MAAPBA) NPs and 20 μL of NaOH aqueous solution (0.1 M) were dispersed in 1 mL of the prepared real samples. With the same operating steps as the complex samples, images of the plates were captured, and the colony count was counted. All the experiments were carried out in triplicate.

Results and discussion

Synthesis and characterization of the Fe_3O_4@poly(PEGDA-*co*-MAAPBA) NPs

The synthetic procedure for the Fe_3O_4@poly(PEGDA-*co*-MAAPBA) NPs is presented in Fig. 1, involving a three-step approach: the synthesis of Fe_3O_4 NPs, the preparation of double-bond functionalized Fe_3O_4 NPs (Fig. 1A), and the copolymerization of Fe_3O_4 NPs, PEGDA, and MAAPBA (Fig. 1B).

To verify the successful synthesis of double-bond functionalized Fe_3O_4 NPs, average particle size analysis was used to investigate the prepared Fe_3O_4 NPs. The particle size distribution and average particle size results showed that the unmodified Fe_3O_4 NPs had the smallest average particle size at 171.0 nm (Fig. 2D), with approximately 70% falling in the range of 122–220 nm (Fig. 2A). After modification with TEOS and TPM, the average particle size of Fe_3O_4 NPs increased from 180.2 nm, with around 70% in the range of 142–255 nm (Fig. 2B), to 195.0 nm, with around 70% in the range of 142–295 nm (Fig. 2C). These results proved that the Fe_3O_4 NPs were successfully modified with double bonds layer by layer, as evidenced by both increased average particle sizes and expanded distributions in particle sizes.

To further confirm the successful synthesis of double-bond functionalized Fe_3O_4 NPs, FTIR spectra (Fig. 2E) and zeta potentials (Fig. 2F) were employed to characterize the functional groups and the charges of the obtained NPs prepared by Step 1. Compared with Fe_3O_4 NPs, the FTIR spectra of Fe_3O_4@SiO_2 and Fe_3O_4@SiO_2@TPM NPs exhibited the presence of two distinct peaks in the region of 900–1300 cm^{-1}. The strong peak at 1070 cm^{-1} was attributed to the Si–O–Si stretching vibrations, and the weak peak at 926 cm^{-1} was ascribed to the Si–OH stretching vibrations.[43,44] There were no obvious differences between the FTIR spectra of Fe_3O_4@SiO_2@TPM NPs and Fe_3O_4@SiO_2, except for the appearance of peaks in the region of 2800–3100 cm^{-1}. These two peaks observed at 2960 cm^{-1} and 2920 cm^{-1} corresponded to the symmetric C–H stretches of methyl ($-CH_3$) groups.[45] These results indicated that the Fe_3O_4 NPs were successfully modified to form double-bond functionalized Fe_3O_4 NPs layer by layer.

According to the synthesis of double-bond functionalized Fe_3O_4 NPs shown in Fig. 1A, the zeta potentials of the prepared

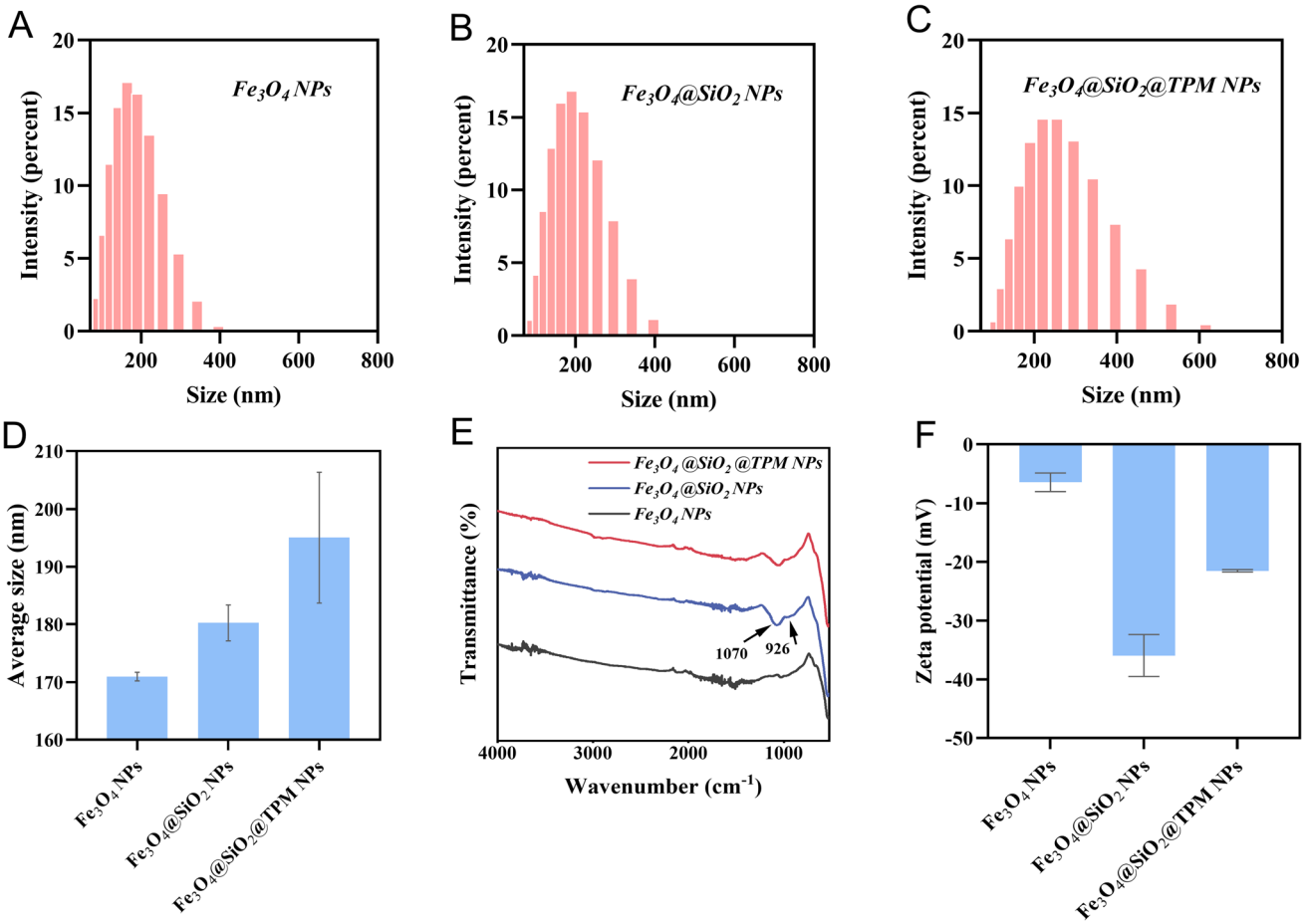

Fig. 2 Characterization of the double-bond functionalized Fe_3O_4 NPs. Particle size distribution of (A) Fe_3O_4 NPs, (B) Fe_3O_4@SiO_2 NPs, and (C) Fe_3O_4@SiO_2@TPM NPs. (D) Average particle size analysis, (E) FTIR spectra, and (F) zeta potentials of Fe_3O_4, Fe_3O_4@SiO_2, and Fe_3O_4@SiO_2@TPM NPs. From Fe_3O_4 to Fe_3O_4@SiO_2@TPM NPs, their particle size distributions increased, and their average particle sizes expanded. In comparison with the FTIR spectrum of Fe_3O_4, Fe_3O_4@SiO_2 NPs appeared two new peaks at 1070 and 926 cm^{-1}, ascribing to the Si–O–Si stretching vibrations, and the Si–OH stretching vibration. In comparison with the FTIR spectrum of Fe_3O_4@SiO_2 NPs, Fe_3O_4@SiO_2@TPM NPs observed two peaks at 2960 and 2920 cm^{-1} corresponding to the symmetric C–H stretches of methyl ($-CH_3$) groups. In comparison with the zeta potential of Fe_3O_4, Fe_3O_4@SiO_2 NPs decreased to -36.71 ± 3.30 mV due to the presence of Si–OH groups on their surface. The zeta potential of Fe_3O_4@SiO_2@TPM NPs increased to -21.52 ± 0.21 mV because of the reduction in Si–OH groups and the increase in double bonds.

Fe_3O_4 NPs should change with the layer-by-layer modification of the silanized surface. As illustrated in Fig. 2F, the Fe_3O_4 NPs were found to have a negatively charged surface (-6.12 ± 1.55 mV) in ultra-pure water. After the modification with TEOS, the zeta potential of the resulting Fe_3O_4@SiO_2 NPs decreased to -36.71 ± 3.30 mV due to the presence of Si–OH groups on their surface. Then, the zeta potential of the double-bond functionalized Fe_3O_4 NPs increased to -21.52 ± 0.21 mV. It could be attributed to the reduction in Si–OH groups and the increase in double bonds. These results further supported that the Fe_3O_4 NPs were successfully modified to form double-bond functionalized Fe_3O_4 NPs layer by layer.

To confirm the successful synthesis of Fe_3O_4@poly(PEGDA-*co*-MAAPBA) NPs, zeta potential, particle size distribution, and CFU counting method were used to characterize and optimize the phenylboronic acid-functionalized NPs. According to the possible reactions between PEGDA, MAAPBA, and Fe_3O_4@SiO_2@TPM NPs shown in Fig. 1B, there are numerous amide groups on the obtained Fe_3O_4@poly(PEGDA-*co*-MAAPBA) NPs. The pH of the solution is an important factor that can greatly affect the surface charge of functionalized NPs. As shown in our previous work, the amide groups functionalized materials could acquire a positive charge at a pH below 6.[46] In this study, the zeta potential measurements in an acidic solution (pH 3) of the synthesized NPs were used to validate the copolymerization process involving PEGDA, MAAPBA, and Fe_3O_4@SiO_2@TPM NPs due to the amide groups introducing from MAAPBA could be protonated in acidic solution. As illustrated in Fig. 3A, the Fe_3O_4@poly(PEGDA) NPs (S1) were found to have a negatively charged surface (-11.30 ± 0.60 mV) in an acidic solution (pH 3). With an increase in the mass ratio of MAAPBA, the zeta potential of the resulting Fe_3O_4@poly(PEGDA-*co*-MAAPBA) NPs rose from -7.37 ± 0.50 mV (S2, MAAPBA to PEGDA mass ratio of 1 : 200) to $+2.85 \pm 0.47$ mV (S5, MAAPBA to PEGDA mass ratio of 1 : 10). These results could be explained by the protonation of extensive amide groups on Fe_3O_4@poly(PEGDA-*co*-MAAPBA)

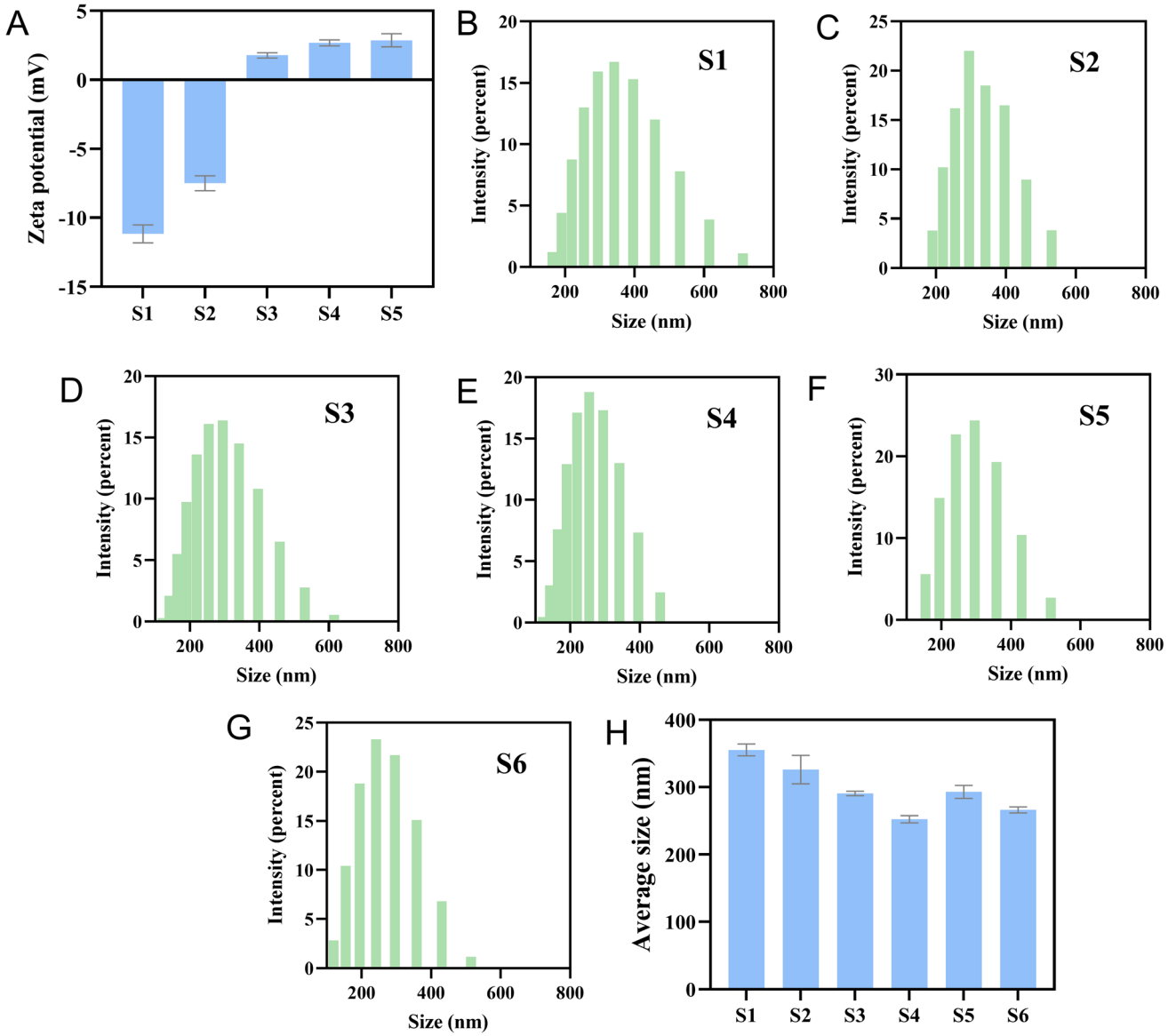

Fig. 3 Characterization of the Fe_3O_4@poly(PEGDA-*co*-MAAPBA) NPs. (A) Zeta potential of the obtained NPs. Particle size distribution of (B) S1, (C) S2, (D) S3, (E) S4, (F) S5, and (G) S6. (H) Average particle size analysis. The zeta potential of Fe_3O_4@poly(PEGDA) NPs (S1) was -11.30 ± 0.60 mV in an acidic solution (pH 3), while Fe_3O_4@poly(PEGDA-*co*-MAAPBA) NPs rose from -7.37 ± 0.50 mV (S2) to $+2.85 \pm 0.47$ mV (S5), due to more and more amide groups appeared on NPs.

NPs in the acidic solution, resulting in an increase in the zeta potential of the resulting NPs. The results of the zeta potential measurements are consistent with the possible chemical reactions, as shown in Fig. 1B, thereby confirming the successful copolymerization between PEGDA, MAAPBA, and Fe_3O_4@SiO_2@TPM NPs.

Due to the strong FTIR absorbance of Fe_3O_4 NPs, the FTIR spectra of poly(PEGDA-*co*-MAAPBA) without Fe_3O_4 NPs were used to confirm the successful copolymerization between PEGDA and MAAPBA (ESI Figure 1†). A series of copolymers with varying MAAPBA to PEGDA mass ratios (1 : 200, 1 : 100, 1 : 50, 1 : 10, and 1 : 5) were synthesized and designated as PS2, PS3, PS4, PS5, and PS6, respectively. The obtained poly(PEGDA) without NPs was named PS1 herein. There were no obvious differences in the FTIR spectra of PS1 and PS2 when compared with that of PS1. With increasing the amount of MAAPBA, two characteristic peaks associated with MAAPBA at approximately 1530 cm^{-1} and 713 cm^{-1} appeared in the spectra of PS4, PS5, and PS6. These peaks were attributed to the flexural vibrations of N–H groups and the benzene ring vibrations.[47] These results proved that MAAPBA could copolymerize with PEDGA to form the capping copolymers of Fe_3O_4@SiO_2@TPM NPs.

Analysis of particle size distributions of the NPs obtained after copolymerization showed that S1 had the largest average particle size of 355.3 nm (Fig. 3H), with approximately 70% in the range of 255–459 nm (Fig. 3B). With increasing the amount of MAAPBA, the average particle size of Fe_3O_4@poly(PEGDA-*co*-MAAPBA) NPs decreased from 325.9 nm (S2), with around 70%

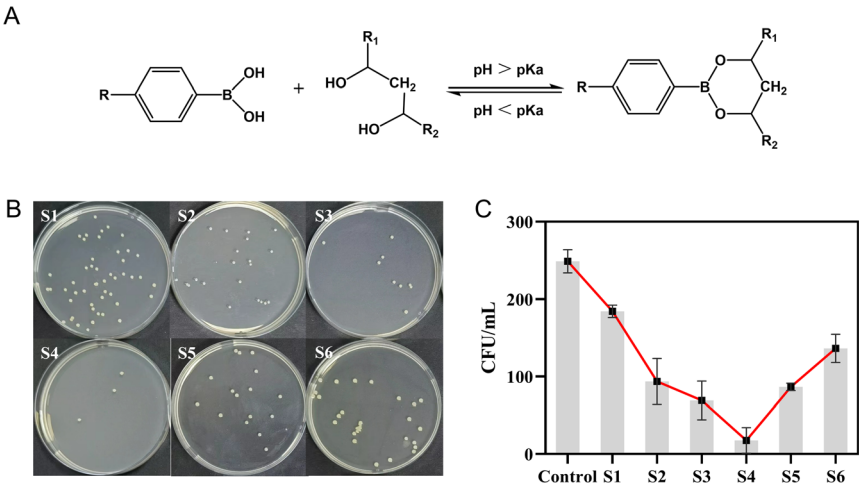

Fig. 4 (A) The reaction mechanism of phenylboronic acid with the *cis*-diol structure of bacteria. When the pH of the surrounding environment exceeds the pK_a value of the boronic acid, the boronic acid engages with *cis*-diols and generates five- or six-membered cyclic esters. As the pH of the surrounding environment switches to acidic, the stable interaction between the Fe_3O_4@poly(PEGDA-*co*-MAAPBA) NPs and bacteria could be dissociated. Consequently, the Fe_3O_4@poly(PEGDA-*co*-MAAPBA) NPs could covalently bind to the peptidoglycan, lipopolysaccharide, and glycoprotein-containing *cis*-diol structure on the surface of bacteria in an alkaline aqueous solution. (B) Image of the plate counting results of *S. aureus* supernatant after treatment with Fe_3O_4@poly(PEGDA-*co*-MAAPBA) NPs. (C) Counting results of *S. aureus* supernatant after treatment with Fe_3O_4@poly(PEGDA-*co*-MAAPBA) NPs. The lowest level of *S. aureus* cells was observed post-introduction of S4 NPs due to the phenylboronic acid groups on the Fe_3O_4 NPs targeting and capturing the *S. aureus*, herein, leaving the least *S. aureus* cells in the supernatant.

in the range of 255–395 nm, to 252.5 nm (S4), with around 70% in the range of 220–342 nm. The observed reduction in average particle sizes and particle size distributions from S1 to S4 suggested that MAAPBA participated in the copolymerization process with PEGDA and Fe_3O_4 NPs, thereby mitigating the self-polymerization of the cross-linker PEGDA. As the mass ratio of MAAPBA to PEGDA was further increased, the average particle size began to fluctuate, and the particle size distribution showed a broadening. This result may be attributed to the mass of MAAPBA in S5 exceeding the maximum one for copolymerization, leading to a more random copolymerization and producing particles with larger average particle sizes and wider particle size distributions. Thus, the optimal mass ratio of MAAPBA to PEGDA was determined to be 1 : 50 (S4), which provided the smallest average particle size, the narrowest particle size distribution, and a relatively high zeta potential (2.68 ± 0.21 mV).

The general reaction mechanism involving the interaction between boronic acid and *cis*-diol-containing compounds is illustrated in Fig. 4A. When the pH of the surrounding environment exceeds the pK_a value of the boronic acid, the boronic acid exists as a tetragonal boronate anion (sp^3) configuration, enabling it to engage with *cis*-diols and generate five- or six-membered cyclic esters.[29] Consequently, the Fe_3O_4@poly(PEGDA-*co*-MAAPBA) NPs could covalently bind to the peptidoglycan, lipopolysaccharide, and glycoprotein-containing *cis*-diol structure on the surface of bacteria in an alkaline aqueous solution. The stable interaction between the Fe_3O_4@poly(PEGDA-*co*-MAAPBA) NPs and bacteria could be dissociated when the environmental pH is switched to acidic. In this study, the CFU counting method was used to further confirm the successful synthesis of Fe_3O_4@poly(PEGDA-*co*-MAAPBA) NPs *via* capturing bacteria in an alkaline aqueous solution and then the left bacteria in the solution were cultured and counted. *S. aureus* (ATCC 29213) was utilized as the model bacterial strain. The concentration of all NPs was fixed at 1 mg mL^{-1}. The CFU results indicated a significant decrease in the quantity of *S. aureus* cells in the supernatant after the addition of Fe_3O_4@poly(PEGDA-*co*-MAAPBA) NPs (Fig. 4B and C). The lowest level of *S. aureus* cells was observed post-introduction of S4 NPs. These results can be explained that the phenylboronic acid groups on the Fe_3O_4 NPs effectively targeted and captured the *S. aureus*, leading to their removal *via* magnetic force and subsequent decrease in cell count within the supernatant. These findings provided additional evidence for the chemical reaction shown in Fig. 1, wherein MAAPBA successfully copolymerized with PEDGA and Fe_3O_4@SiO_2@TPM NPs to form the Fe_3O_4@poly(PEGDA-*co*-MAAPBA) NPs containing numerous phenylboronic acid groups. Moreover, the reduced capture of *S. aureus* by S5 compared to S4 further supported the notion that the optimal copolymerization ratio was 1 : 50, that is, the highest mass of MAAPBA participated in the copolymerization reaction to form the most phenylboronic acid groups on Fe_3O_4@SiO_2@TPM NPs, producing the largest recognition of *S. aureus* cells, the smallest average particle size, narrowest particle size distribution, and relatively high surface charge. Consequently, the S4 was utilized in all subsequent experiments.

Selectivity

The selectivity of S4 to bacteria was examined through analysis of changes in turbidity values of *E. coli* (Gram-negative) and *S. aureus* (Gram-positive), quantification of CFU counts, and SEM images. Specifically, varying amounts of S4 were added to *E. coli* or *S. aureus* PBS suspension (approximately 1×10^8 CFU mL^{-1}),

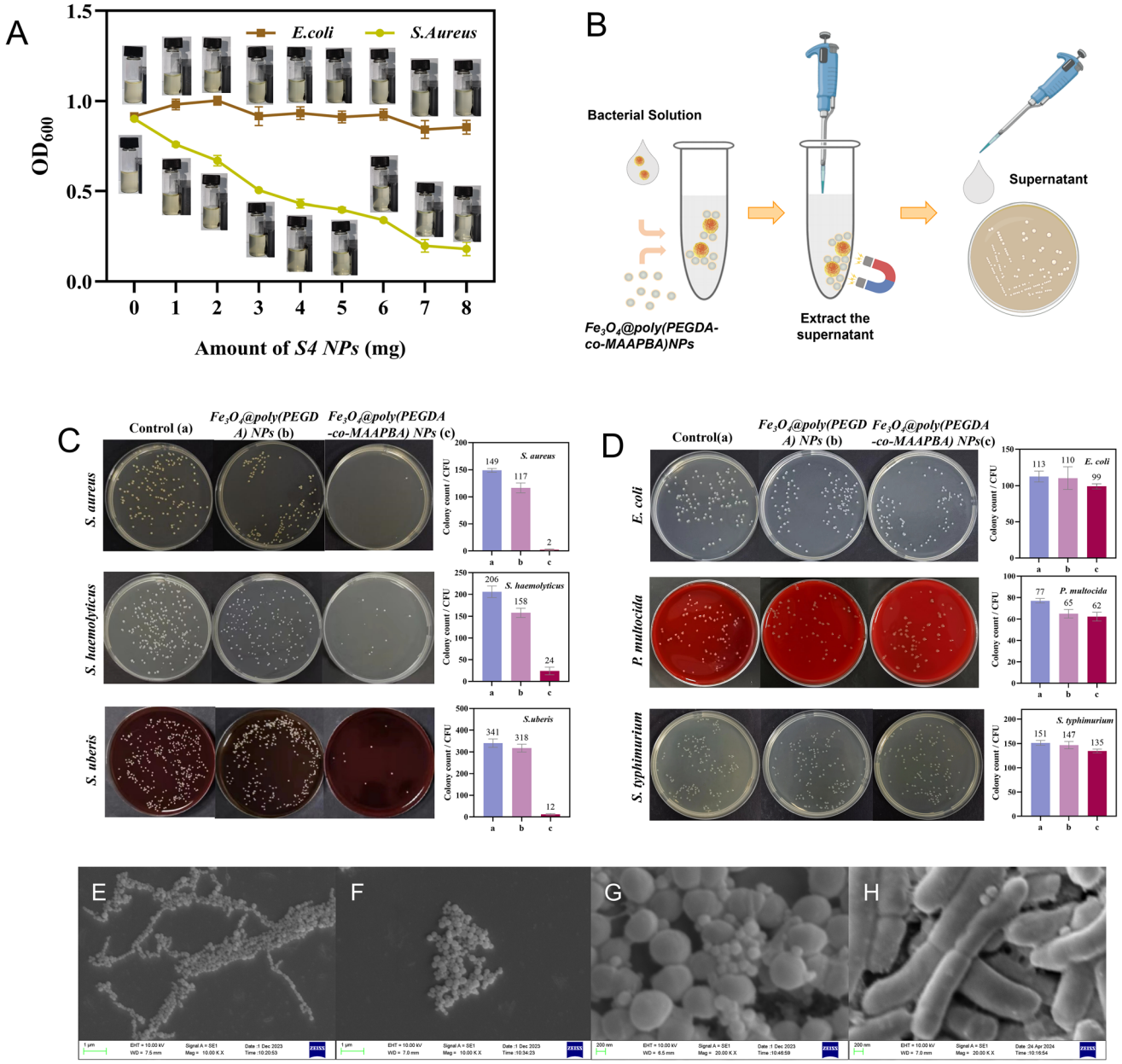

Fig. 5 (A) The curve of turbidity changes with the addition of S4 NPs from 0 to 8 mg. With the mass of S4 increasing from 0 to 8 mg, the turbidity values of the *S. aureus* PBS suspensions decrease accordingly. There was no obvious difference in *E. coli* PBS suspensions with increasing mass of S4. (B) The procedure of S4 captures bacteria and determines the number of bacteria left in the suspension using the plate culture. Images of the plate counting results of bacteria supernatant after treatment with Fe_3O_4@poly(PEGDA) NPs or Fe_3O_4@poly(PEGDA-*co*-MAAPBA) NPs. (C) Gram-positive bacteria, and (D) Gram-negative bacteria. The numbers of three Gram-positive bacteria following treatment with S4 were significantly less than the control groups of bacteria solution without NPs treatment, while there were no obvious changes in the numbers of Gram-negative bacteria after the treatment with S4. SEM images of (E) Fe_3O_4 NPs, (F) Fe_3O_4@poly(PEGDA-*co*-MAAPBA) NPs, (G) the surface of *S. aureus* cells in the presence of Fe_3O_4@poly(PEGDA-*co*-MAAPBA) NPs, and (H) the surface of *E. coli* cells in the presence of Fe_3O_4@poly(PEGDA-*co*-MAAPBA) NPs. After treatment with *E. coli* or *S. aureus* suspension, some S4 NPs attached to *S. aureus* cells, while almost no S4 was present on the *E. coli* cells. These results proved a selectivity of S4 for Gram-positive bacteria, attributing to the higher content of peptidoglycan in the cell wall of Gram-positive bacteria.

followed by magnetic capture of the bacteria. Fig. 5A showed a decrease in turbidity values for the *S. aureus* PBS suspensions with the amount of S4 increasing from 0 to 8 mg. In contrast, no such decrease was observed in the *E. coli* PBS suspensions with increasing amounts of S4. These results indicated a selectivity of S4 for *S. aureus* (Gram-positive bacteria), attributed to the higher content of peptidoglycan in the cell wall of Gram-positive bacteria.

The selectivity of S4 towards Gram-positive bacteria was confirmed using the CFU counting method to determine the

number of bacteria in the suspension after treatment with 1 mg of S4. The corresponding procedure of S4 captures bacteria and determines the number of bacteria left in the suspension as illustrated in Fig. 5B. Gram-negative bacteria (*E. coli*, *S. typhimurium*, and *P. multocida*) and Gram-positive bacteria (*S. aureus*, *S. haemolyticus*, and *S. uberis*) were chosen as the model bacteria. As shown in Fig. 5C, the numbers of three Gram-positive bacteria following treatment with S4 were significantly lower than the control groups of bacteria solution without NPs treatment. In comparison with the Gram-negative bacteria solution without the treatment of NPs, there were no obvious changes in the numbers of *E. coli*, *S. typhimurium*, or *P. multocida* after the treatment with S4 (Fig. 5D). Additionally, the numbers of Gram-positive or Gram-negative bacteria following treatment with S1 were similar to the control groups of bacteria solution without NP treatment. These results indicated that S1 exhibited minimal non-specific selectivity for bacteria. The obvious distinction between the recognition of Gram-positive and Gram-negative bacteria suggested that S4 had a remarkable selectivity for Gram-positive bacteria, which was consistent with the results of turbidity values presented in Fig. 5A.

To further demonstrate the selectivity of S4 on Gram-positive bacteria, SEM images were utilized to directly observe the impact on the surface of *E. coli* and *S. aureus* cells in the presence of S4. The results revealed that the Fe_3O_4 NPs exhibited a uniform size at around 200 nm with a spherical shape, while after copolymerization with MAAPBA and PEDGA, S4 displayed a uniform spherical size at around 300 nm (Fig. 5E and F). Subsequent treatment with *E. coli* or *S. aureus* suspension for 30 min at 37 °C demonstrated the presence of some S4 NPs on the surface of *S. aureus* cells (Fig. 5G). On the contrary, there was no S4 present on the surface of *E. coli* cells (Fig. 5H). These results further proved that the Fe_3O_4@poly(PEGDA-*co*-MAAPBA) NPs had excellent selective recognition for Gram-positive bacteria.

Live/dead staining test

To ascertain the viability of bacteria anchored by S4, a combination of fluorescence live/dead staining measurements and the CFU counting method was employed to view the bacterial condition. As shown in Fig. 6A, *S. aureus* exhibited robust activity prior to treatment with S4 because of the presence of green fluorescence only. After the treatment with S4 for 15 min, there were only a few red fluorescent dots, indicating that most of the bacteria were live bacteria (Fig. 6B). Concurrently, two prominent clusters of green fluorescence emerged, suggesting that S4 NPs recognized *S. aureus* and agglomerated into the larger fluorescent spots (Fig. 6C). These results showed that the bacteria anchored by the Fe_3O_4@poly(PEGDA-*co*-MAAPBA) NPs

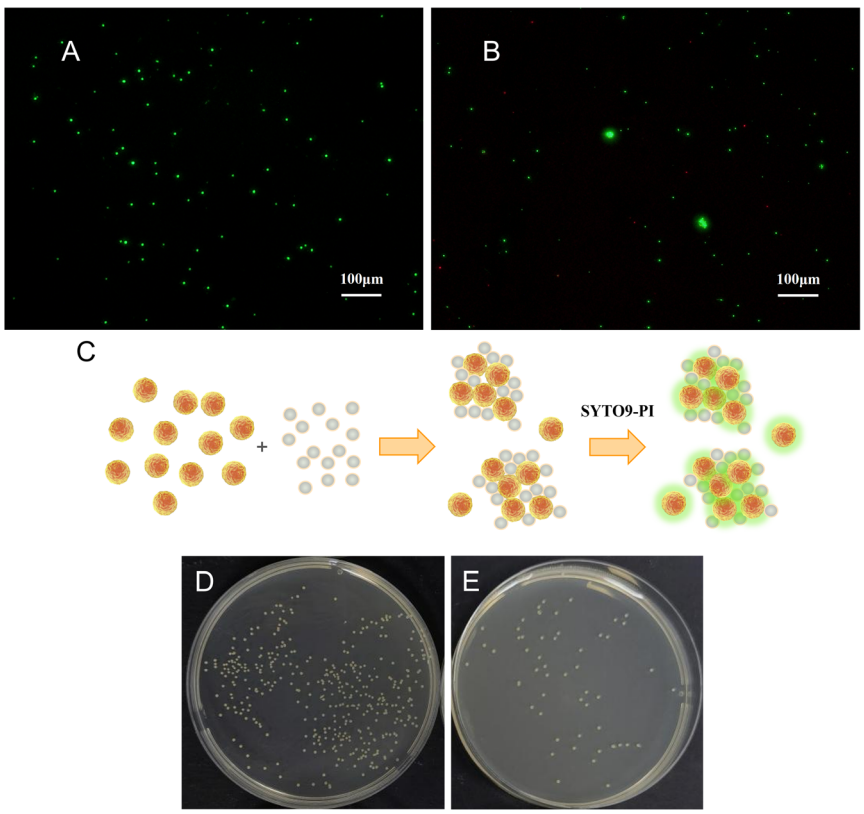

Fig. 6 Fluorescence microscope images of bacteria. (A) The suspensions of *S. aureus*. (B) Fe_3O_4@poly(PEGDA-*co*-MAAPBA) NPs were added to suspensions of *S. aureus*. (C) The possible mechanism for Fe_3O_4@poly(PEGDA-*co*-MAAPBA) NPs recognizing *S. aureus* and agglomerating to form the larger green fluorescence clusters. A good deal of *S. aureus* was cultured in the S4 NPs group (D), while only a few *S. aureus* strains appeared in the control group (E).

were live strains, facilitating their direct cultivation with S4 for bacterial diagnostic purposes. Subsequent to a 24 hour cultivation period, there was a good deal of *S. aureus* cultured in the S4 group, in contrast to the minimal presence of *S. aureus* strains in the control group (Fig. 6D and E). These results provided further validation of the live-straining nature of bacteria anchored by S4, and their potential for diagnostic culture. Additionally, the increased numbers of *S. aureus* in the S4 group suggested the effective enrichment capability of Fe_3O_4@poly(PEGDA-*co*-MAAPBA) NPs for low concentrations of *S. aureus*.

Enrichment capability and reusability

The enrichment capability of the Fe_3O_4@poly(PEGDA-*co*-MAAPBA) NPs was assessed using the CFU counting method, wherein S4 NPs were cultured directly for 24 h following the capture of *S. aureus*, *S. haemolyticus*, or *Staphylococcus*, to count the number of corresponding bacteria. The corresponding procedure for S4 NPs involves the capture of bacteria, followed by the determination of the number of bacteria on the NPs, as illustrated in Fig. 7A. Compared with the initial low-concentration bacterial solution (control), all groups treated with S4 showed obvious boosting numbers of cultured bacteria

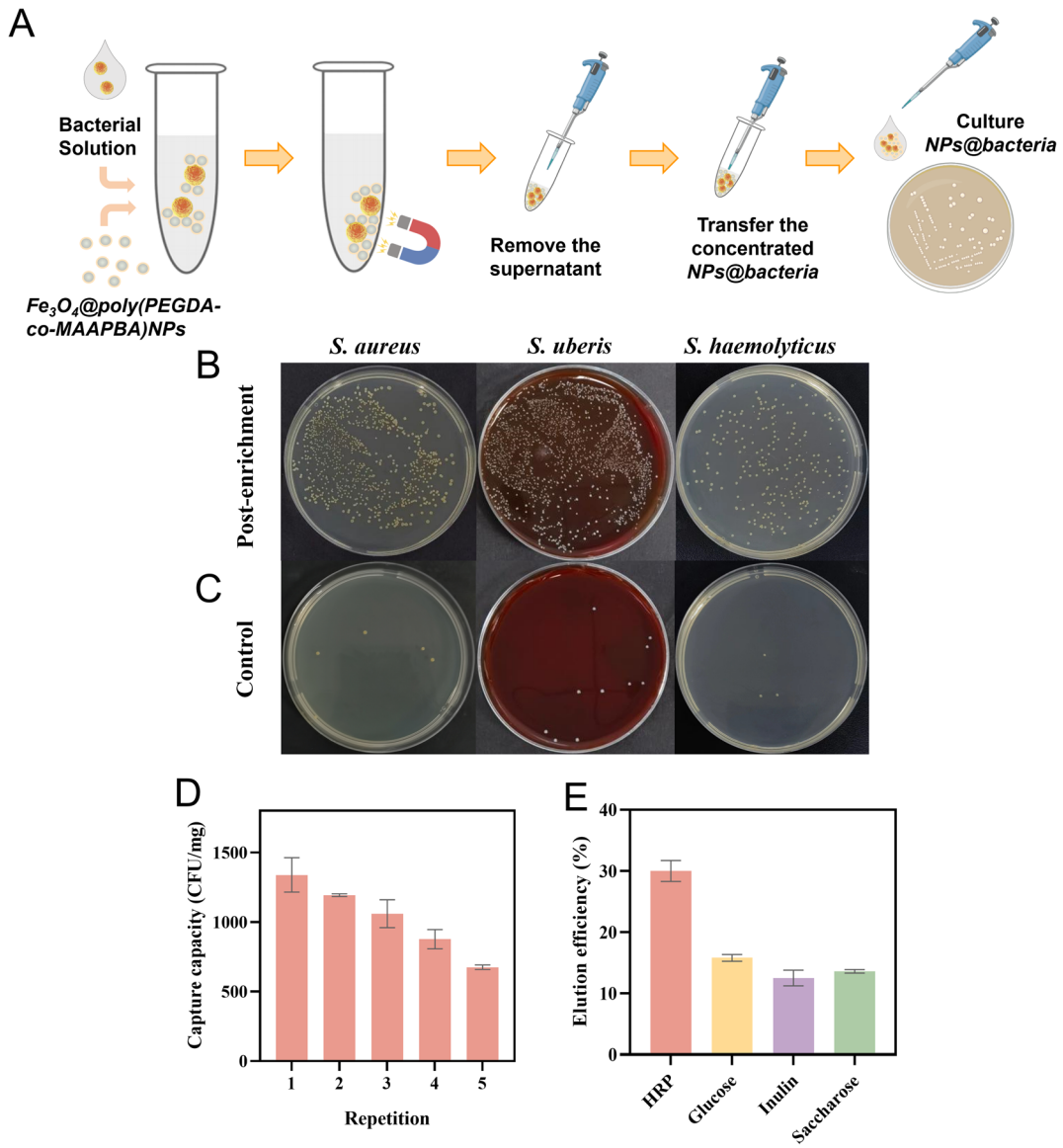

Fig. 7 (A) The procedure of S4 captures bacteria and determines the number of bacteria on the NPs using the plate culture. Images of the plate counting results of (B) bacterial solution without treatment with S4 NPs, and (C) S4 were cultured directly for 24 h following the capture of Gram-positive bacteria. Compared with the initial low-concentration bacterial solution (control), all groups treated with S4 showed obvious boosting numbers of cultured bacteria. (D) The reusability of S4 NPs. After the fifth cycle, the capture capacity of *S. aureus* decreased from 1.34×10^3 CFU mg^{-1} to 6.75×10^2 CFU mg^{-1}. (E) Elution efficiency of some moderate eluents. The elution rates are 30.0%, 15.8%, 12.5%, and 13.6% for HRP, glucose, inulin, and saccharose, respectively. The different elution rates may be attributed to the difference in affinity between boronate affinity materials and the eluents.

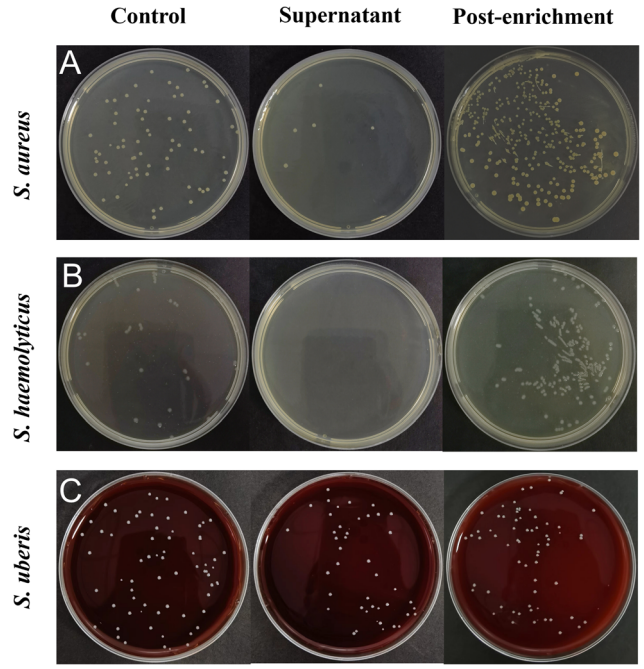

Fig. 8 The enrichment capacity of Fe_3O_4@poly(PEGDA-*co*-MAAPBA) NPs for Gram-positive bacteria in intestinal fluid. Image of the plate counting results of (A) *S. aureus*, (B) *S. haemolyticus*, and (C) *S. uberis*n. Compared with the original low-concentration bacterial intestinal fluid (control), all groups treated with S4 NPs exhibited a notable increase.

(Fig. 7B and C). The enrichment capabilities of S4 NPs to *S. aureus*, *S. haemolyticus*, and *Staphylococcus* were found to be 266.5, 246, and 318.2 times, respectively. It presents the LOD of the microbiological culture method was reduced from 30 CFU mL^{-1} to 0.1 CFU mL^{-1} after treatment with S4 NPs. The results proved that the prepared Fe_3O_4@poly(PEGDA-*co*-MAAPBA) NPs were capable of detecting low concentrations of pathogenic bacteria by enriching live bacteria and then determining them by conventional diagnostic methods.

The reusability of functional NPs is important for their application in the detection of bacteria. Acetic acid solutions are conventionally employed to dissociate *cis*-diol-containing compounds bound by phenylboronic acid ligands. Therefore, the reusability of the Fe_3O_4@poly(PEGDA-*co*-MAAPBA) NPs was evaluated through multiple capture-dissociation cycles using an acetic acid solution and the established capture process. The concentration of S4 was set at 0.6 mg mL^{-1}, and a standard solution of *S. aureus* at a concentration of 1×10^3 CFU mL^{-1} was used as the model bacterial solution. After the third cycle, the capture capacity of *S. aureus* decreased from 1.34×10^3 CFU mg^{-1} to 1.06×10^3 CFU mg^{-1}, representing a 20.89% decrease. Even to the fifth cycle, the capture capacity reached 6.75×10^2 CFU mg^{-1}. Despite this loss, the results suggested that the Fe_3O_4@poly(PEGDA-*co*-MAAPBA) NPs remained stable and could be readily reused. It is crucial to note that, given the necessity for dissociated bacteria to be cultured for diagnostic purpose, some

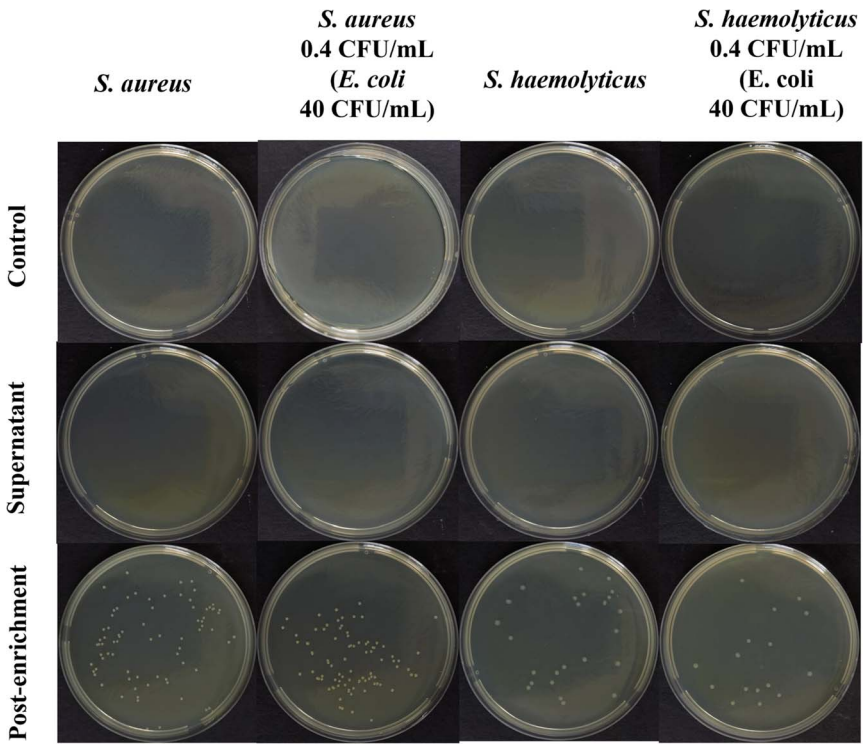

Fig. 9 The enrichment capability and selectivity of Fe_3O_4@poly(PEGDA-*co*-MAAPBA) NPs for *S. aureus* (approximately 0.4 CFU mL^{-1}) or *S. haemolyticus* (approximately 0.4 CFU mL^{-1}) in urine containing *E. coli* (approximately 40 CFU mL^{-1}). There were no bacterial cells observed in the prepared urine samples (control), indicating the invalidity of the conventional culture-based method for determining low-concentration pathogenic bacteria. By contrast, all groups treated with S4 NPs showed obvious boosting numbers of cultured *S. aureus* and *S. haemolyticus*, suggesting the superior selectivity and enrichment capability of the NPs in real and complex samples.

Table 1 Extraction and detection of bacteria with nanomaterials

NPs	Recognition elements	Specificity	Model bacteria	Samples	Detection method	LOD (CFU mL^{-1})	Reusable	Ref.
Fe_3O_4@PDA@Pd/Pt	Antibody	Yes	E. coli O157:H7	Milk	Lateral flow assay	9×10^1	No	19
Pt–PCN-224	Antibody	Yes	E. coli O157:H7	Water, milk, and cabbage	Microfluidic biosensor	10^3	No	17
IFMNBs	Antibody	Yes	E. coli O157:H7	Milk	Lateral flow assay	2.5×10^3	No	48
PtNP@Van	Antibiotic	Yes	Gram-positive bacteria	Grape juice Skimmed milk Tap water	Filter discoloration	30.3 ± 2.5 47 ± 3.6 92.7 ± 3.2	No	8
GO-PEI	Positive charge	No	*E. coli* O157:H7	Milk	Colorimetric method	24	No	49
UAA@P/M NPs	Boric acid group	Unmentioned	*S. aureus*	5% diluted human serum	Lateral flow immunoassay strip	10^2	No	50
UiO-66-$B(OH)_2$		Unmentioned	*E. coli*	—	Fluorescence colorimetry	1	No	27
MOF@COFBA		Unmentioned	*S. aureus*, *Acinetobacter baumannii*	Normal human serum, urine, and cerebrospinal fluid	Fluorescence colorimetry	7 5	No	24
Au-PMBA		Unmentioned	*S. aureus*, *E. coli*	Potable water, watermelon juice, milk, and beef	Lateral flow immunoassay strip	10^3	No	29
Fe_3O_4@poly(PEGDA-*co*-MAAPBA) NPs		Yes	Gram-positive bacteria	Artificial intestinal fluid Urine	Culture method	0.4	Yes	This work

moderate eluents were examined in this work to dissociate bacteria from the Fe_3O_4@poly(PEGDA-*co*-MAAPBA) NPs without compromising bacterial activity. The boronate affinity NPs have higher binding strength towards HRP, glucose, inulin, and saccharose. Thus, in this work, 1 mL of HRP, glucose, inulin, or saccharose aqueous solution (0.3 mg mL^{-1}, pH = 7.4) was used as the eluent to dissociate bacteria from S4. As shown in Fig. 7E, the elution rate of the HRP solution reached 30.0%, which was higher than that of glucose (15.8%), inulin (12.5%), and saccharose (13.6%). These results may be attributed to the different affinity of boronate affinity materials to HRP, glucose, inulin, and saccharose. Considering the elution rate and certain reusability, the optimal method for utilizing S4 involves initially capturing bacteria, followed by direct culturing of the S4 NPs for diagnosis. Then, acetic acid solution can be employed to dissociate bacteria for the reuse of S4 NPs.

Detection of Gram-positive bacteria in complex samples

In this study, the prepared Fe_3O_4@poly(PEGDA-*co*-MAAPBA) NPs demonstrated notable selectivity toward Gram-positive bacteria, thus motivating their utilization for the capture of Gram-positive bacteria from complex samples. First, *S. aureus*, *S. haemolyticus*, or *S. uberis* was introduced into the sterile intestinal fluid to generate a complex sample. The capture efficiency of S4 was determined through the CFU counting method. Compared with the original low-concentration bacterial intestinal fluid (control), all groups treated with S4 NPs exhibited a significant increase in these cultured bacteria (Fig. 8A–C). The enrichment capabilities of S4 for *S. aureus*, *S. haemolyticus*, and *Staphylococcus* in the intestinal fluid were 118.3, 193.8, and 20.6 times, respectively. The results proved that the prepared Fe_3O_4@poly(PEGDA-*co*-MAAPBA) NPs possessed both excellent selectivity and enrichment capability for detecting low-concentration Gram-positive bacteria in intestinal fluid.

Subsequently, *S. aureus* or *S. haemolyticus* suspension (approximately 10^2 CFU mL^{-1}) and *E. coli* suspension (approximately 10^4 CFU mL^{-1}) were diluted with the urine collected from a female volunteer to simulate a real bacterial sample with a concentration of approximately 0.4 CFU mL^{-1} of *S. aureus* or *S. haemolyticus* and 40 CFU mL^{-1} of *E. coli*. These urine samples are considered healthy samples during routine urinary examinations. The enrichment capability and selectivity of the S4 NPs in real samples were assessed using the CFU counting method, wherein S4 NPs were cultured directly for 24 h following the capture of bacteria from the prepared urine samples. As shown in Fig. 9, no bacterial cells were observed in the prepared urine samples, indicating the invalidity of the conventional culture-based method for low-concentration pathogenic bacteria. In contrast, all groups treated with S4 NPs exhibited a notable increase in these cultured bacteria, even in urine samples with the presence of abundant competing bacteria *E. coli* (100-fold). These results further validated the superior selectivity and enrichment capability of the Fe_3O_4@poly(PEGDA-*co*-MAAPBA) NPs for detecting low-concentration pathogenic bacteria in real and complex samples.

In comparison to the recently reported methods for bacterial extraction with nanomaterials, the Fe_3O_4@poly(PEGDA-*co*-MAAPBA) NPs reveal the superior performance. For example, the sensitivity is enhanced even when combined with the culture method, and the reusability is more satisfactory (Table 1). Despite the absence of specificity for particular bacteria, the Fe_3O_4@poly(PEGDA-*co*-MAAPBA) NPs show excellent selective recognition for Gram-positive bacteria. Furthermore, as a non-immune and label-free nanomaterial, the Fe_3O_4@poly(PEGDA-*co*-MAAPBA) NPs offer some inherent advantages, such as excellent tolerance against acid or base, reduced costs, and no stringent requirements for storage conditions. These results collectively underscore the promising utility of Fe_3O_4@poly(PEGDA-*co*-MAAPBA) NPs in the detection of low-concentration Gram-positive pathogens in real and complex samples.

Conclusions

In the present work, phenylboronic acid-functionalized Fe_3O_4 NPs were developed to enrich low abundances of pathogenic bacteria from complex biological samples and detect them with high sensitivity. The Fe_3O_4 NPs were prepared by a solvothermal method and then modified through silanization to introduce double bonds. Following copolymerization with the phenylboronic acid functional monomer MAAPBA and cross-linker PEGDA, Fe_3O_4@poly(PEGDA-*co*-MAAPBA) NPs were synthesized successfully. The resultant Fe_3O_4@poly(PEGDA-*co*-MAAPBA) NPs have demonstrated the ability to capture and dissociate pathogenic bacteria by engaging in reversible reactions between the phenylboronic acid groups on the NPs and the *cis*-diol structures present on the outside of the bacterial cells. The bacteria anchored on the Fe_3O_4@poly(PEGDA-*co*-MAAPBA) NPs remained viable and could be cultured for diagnosis, with an LOD of 0.4 CFU mL^{-1}. The Fe_3O_4@poly(PEGDA-*co*-MAAPBA) NPs were applied successfully for the enrichment and detection of *S. aureus* and *S. haemolyticus* in urine samples which were typically considered to be free of pathogens according to the clinical threshold. Summarily, the poly(-PEGDA-*co*-MAAPBA) @Fe_3O_4 NPs exhibited significant bacterial enrichment capabilities and good reusability, which would effectively improve the sensitivity of classical diagnostic methods.

Data availability

The authors confirm that the data supporting the findings of this study are available within the article [and/or] as its ESI.†

Author contributions

Jingwen Chen: methodology, investigation, and data curation. Shaobo Li: investigation, and data curation. Bin Deng: validation, and data curation. Hongyuan Wang: methodology, and data curation. Wenkui Sun: supporting technology. Li Li: writing original draft-review & editing, supervision, funding acquisition, and conceptualization. Zongchun Bai: funding

acquisition, and supervision. Jing Liu: revising manuscript, supervision, and funding acquisition.

Conflicts of interest

The authors declare that they have no known competing financial interests or personal relationships that could have appeared to influence the work reported in this paper.

Acknowledgements

We would like to express our gratitude to Ziyuan Wang of the Center for Analysis and Testing, China Pharmaceutical University, for her assistance with the instrumentation. This work was financially supported by the Jiangsu Provincial Science and Technology Plan Special Fund Key R&D Plan Social Development Project (BE2023841), the Six Talent Peaks Project of Jiangsu Province, China (Grant No. NY-034), and Jiangsu Agricultural Science and Technology Innovation Fund (Grant No. CX (22)1008).

References

1 D. Bogaert and W. Van Schaik, *Gut*, 2024, **73**, 883–884.
2 W. Chen, M. Li, Z. Chen, Z. Yan, J. Li, L. Guo, C. Ding and Y. Huang, *Biosens. Bioelectron.*, 2023, **234**, 115344.
3 W. C. Hu, J. Pang, S. Biswas, K. Wang, C. Wang and X. H. Xia, *Anal. Chem.*, 2021, **93**, 8544–8552.
4 X. Tao, L. Yue, T. Tian, Y. Zhang, X. Zhou and E. Song, *Anal. Chem.*, 2024, **96**, 9270–9277.
5 Y. X. Liang, Y. K. Wang, W. J. Meng, Q. Wang, J. X. Li, W. H. Huang and M. Xie, *Anal. Chem.*, 2024, **96**, 10013–10020.
6 S. He, Y. Chen, J. Wang, J. Sun, X. Zhang and Q. Chen, *Anal. Chem.*, 2024, **96**, 11018–11025.
7 L. Hu, M. Rossetti, J. F. Bergua, C. Parolo, R. Alvarez-Diduk, L. Rivas, A. Idili and A. Merkoci, *ACS Appl. Mater. Interfaces*, 2024, **16**, 30636–30647.
8 Z. Huang, X. Li, Y. Feng, Y. Tian and Y. Duan, *Sens. Actuators, B*, 2023, **387**, 133817.
9 A. Zhu, T. Jiao, S. Ali, Y. Xu, Q. Ouyang and Q. Chen, *Anal. Chem.*, 2021, **93**, 9788–9796.
10 K. H. Kim, S. J. Park, C. S. Park, S. E. Seo, J. Lee, J. Kim, S. H. Lee, S. Lee, J. S. Kim, C. M. Ryu, D. Yong, H. Yoon, H. S. Song, S. H. Lee and O. S. Kwon, *Biosens. Bioelectron.*, 2020, **167**, 112514.
11 S. Lee, V. S. L. Khoo, C. A. D. Medriano, T. Lee, S. Y. Park and S. Bae, *Water Res.*, 2019, **160**, 371–379.
12 H. Han, B. Sohn, J. Choi and S. Jeon, *Biomed. Eng. Lett.*, 2021, **11**, 297–307.
13 Y. Shen, Y. Zhang, Z. Gao, Y. Ye, Q. Wu, H. Chen and J. Xu, *Nano Today*, 2021, **38**, 101121.
14 G. Wu, H. Qiu, X. Liu, P. Luo, Y. Wu and Y. Shen, *Trends Food Sci. Technol.*, 2023, **142**, 104214.
15 J. Cheon, J. Qin, L. P. Lee and H. Lee, *Acc. Chem. Res.*, 2022, **55**, 121–122.
16 X. Yue, Q. Liao, H. He, H. Li, J. Xie and Z. Fu, *Anal. Chem.*, 2023, **95**, 3754–3760.
17 G. Xing, Y. Shang, J. Ai, H. Lin, Z. Wu, Q. Zhang, J. M. Lin, Q. Pu and L. Lin, *Anal. Chem.*, 2023, **95**, 13391–13399.
18 C. Wang, S. Sun, P. Wang, H. Zhao and W. Li, *Talanta*, 2024, **269**, 125462.
19 X. Huang, G. Zhang, L. Zeng, X. Xiao, J. Peng, P. Guo, W. Zhang and W. Lai, *ACS Appl. Mater. Interfaces*, 2021, **13**, 1413–1423.
20 A. L. Bole and P. Manesiotis, *Adv. Mater.*, 2016, **28**, 5349–5366.
21 L. Wang, W. Qi, M. Wang, F. Jiang, Y. Ding, X. Xi, M. Liao, Y. Li and J. Lin, *Biosens. Bioelectron.*, 2022, **218**, 114765.
22 Y. Liu, L. Wang, H. Li, L. Zhao, Y. Ma, Y. Zhang, J. Liu and Y. Wei, *Prog. Polym. Sci.*, 2024, **150**, 101790.
23 P. Wu, W. Zuo, Y. Wang, Q. Yuan, J. Yang, X. Liu, H. Jiang, J. Dai, F. Xue and Y. Ju, *Chem. Eng. J.*, 2023, **451**, 139021.
24 R. Li, J. Yan, B. Feng, M. Sun, C. Ding, H. Shen, J. Zhu and S. Yu, *ACS Appl. Mater. Interfaces*, 2023, **15**, 18663–18671.
25 Z. Wang, X. Feng, F. Xiao, X. Bai, Q. Xu and H. Xu, *Microchem. J.*, 2022, **178**, 107379.
26 M. Chen, J. Zhang, J. Qi, R. Dong, H. Liu, D. Wu, H. Shao and X. Jiang, *ACS Nano*, 2022, **16**, 7732–7744.
27 W. Zuo, L. Liang, F. Ye and S. Zhao, *Sens. Actuators, B*, 2021, **345**, 130345.
28 J. Y. Yang, X. D. Jia, R. X. Gao, M. L. Chen, T. Yang and J. H. Wang, *Sens. Actuators, B*, 2021, **340**, 129951.
29 P. Wu, F. Xue, W. Zuo, J. Yang, X. Liu, H. Jiang, J. Dai and Y. Ju, *Anal. Chem.*, 2022, **94**, 4277–4285.
30 C. Rong, H. Chen, Z. Wang, S. Zhao, D. Dong, J. Qu, N. Zheng, H. Liu and X. Hua, *J. Hazard. Mater.*, 2024, **466**, 133533.
31 J. Wang, Y. Chen, J. Song, B. Guo, F. Xia, Y. Wan, W. Wu, C. Zhang, S. Feng and M. Wu, *Adv. Funct. Mater.*, 2023, **34**, 2312162.
32 T. Tao, Z. Li, S. Xu, S. U. Rehman, R. Chen, H. Xu, H. Xia, J. Zhang, H. Zhao, J. Wang and K. Ma, *Anal. Chem.*, 2023, **95**, 11542–11549.
33 J. Zhao, Y. Li, X. Chen, D. Mu, J. Zhao and S. Zhou, *Anal. Chem.*, 2022, **95**, 955–965.
34 C. Zhao, X. Jian, Z. Gao and Y. Y. Song, *Anal. Chem.*, 2022, **94**, 14038–14046.
35 F. Wei, X. Cui, Z. Wang, C. Dong, J. Li and X. Han, *Chem. Eng. J.*, 2021, **408**, 127240.
36 M. Shao, F. Ning, J. Zhao, M. Wei, D. G. Evans and X. Duan, *J. Am. Chem. Soc.*, 2012, **134**, 1071–1077.
37 E. R. Ghomi, S. N. Khorasani, M. K. Kichi, M. Dinari, S. Ataei, M. H. Enayati, M. S. Koochaki and R. E. Neisiany, *Colloid Polym. Sci.*, 2020, **298**, 213–223.
38 N. S. Kwak, J. R. Yang, C. W. Hwang and T. S. Hwang, *Chem. Eng. J.*, 2013, **223**, 216–223.
39 S. Rajpal, S. Bhakta and P. Mishra, *J. Mater. Chem. B*, 2021, **9**, 2436–2446.
40 L. Li, Y. Lu, Z. Bie, H. Chen and Z. Liu, *Angew. Chem., Int. Ed.*, 2017, **56**, 2827.

41 J. Bezdekova, K. Zemankova, J. Hutarova, S. Kociova, K. Smerkova, V. Adam and M. Vaculovicova, *Food Chem.*, 2020, **321**, 126673.
42 B. Zheng, M. Guo, Y. Bai, S. Wang, B. Li, Y. Gu, B. Hou, T. Wang and D. Ming, *Mater. Today Adv.*, 2021, **11**, 100147.
43 C. Sarkar, J. K. Basu and A. N. Samanta, *Chem. Eng. J.*, 2019, **377**, 119621.
44 X. Yu, J. Zhang, X. Wang, Q. Ma, X. Gao, H. Xia, X. Lai, S. Fan and T. S. Zhao, *Appl. Catal., B*, 2018, **232**, 420–428.
45 X. Liu, W. Qi, Y. Wang, R. Su and Z. He, *Nanoscale*, 2017, **9**, 17561–17570.
46 S. Zhang, J. Gu, B. Fan, L. Li and B. Li, *Cellulose*, 2022, **29**, 5511–5527.
47 X. Liao, B. Wu, H. Li, M. Zhang, M. Cai, B. Lang, Z. Wu, F. Wang, J. Sun, P. Zhou, H. Chen, D. Di, C. Ren and H. Zhang, *Anal. Chem.*, 2023, **95**, 14573–14581.
48 Z. Huang, J. Peng, J. Han, G. Zhang, Y. Huang, M. Duan, D. Liu, Y. Xiong, S. Xia and W. Lai, *Food Chem.*, 2019, **276**, 333–341.
49 F. Chen, D. Chen, T. Deng and J. Li, *Biosens. Bioelectron.*, 2022, **216**, 114611.
50 X. Huang, L. Chen, W. Zhi, R. Zeng, G. Ji, H. Cai, J. Xu, J. Wang, S. Chen, Y. Tang, J. Zhang, H. Zhou and P. Sun, *Anal. Chem.*, 2023, **95**, 13101–13112.